

## **Part I**

### **Principles and Methods**



## 1

## Introduction

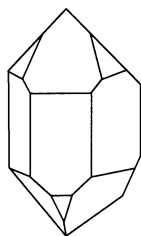
## 1.1

## Crystals and Symmetry

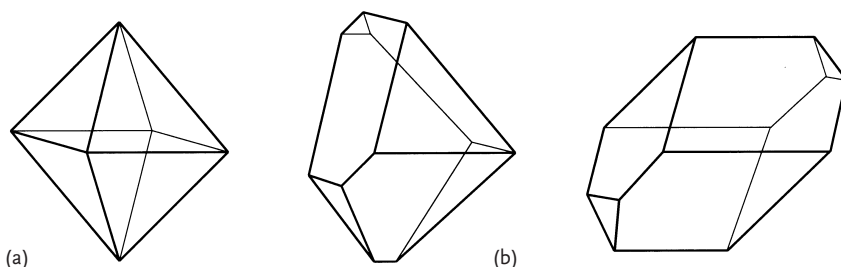
Who has not been fascinated by the regular shape of single crystals of minerals, gemstones, other inorganic compounds and organic substances? Yet, most biological macromolecules can also be crystallized. A characteristic of the so-called morphology of crystals is a set of flat faces, forming a closed body. Figure 1.1 shows a regularly shaped quartz crystal, but the shape may also be skewed, as depicted in Figure 1.2, for lodestone (magnetite,  $\text{Fe}_3\text{O}_4$ ).

It was first shown by Nicolaus Steno (in 1669) that the angles between the faces are constant, independently of the regularity of a given crystal morphology. The analysis of crystal morphologies led to the formulation of a complete set of 32 symmetry classes – also called “point groups” – which all crystal morphologies obey. Possible symmetry elements are 1-, 2-, 3-, 4-, and 6-fold rotations, mirror plane  $m$ , inversion center and a combination of rotation axis with inversion center (inversion axis). As explained later, crystals of biological macromolecules can contain rotation symmetries only, thereby reducing the possible point groups to the 11 enantiomeric point groups: 1, 2, 3, 4, 6, 222, 32, 422, 622, 23, and 432. A graphical representation of the symmetries and of their general morphological crystal form is displayed in Figure 1.3.

The morphology of a crystal tells us much about its symmetry, but little about its internal structure. Before the discovery of X-ray diffraction of crystals by von Laue, Knipping and Friedrich in 1912, it had been proven that crystals are built up from atoms or molecules arranged in a three-dimensionally periodic



**Fig. 1.1** Regularly shaped quartz crystal.



**Fig. 1.2** Different forms of the octahedron of lodestone.  
(a) Regular shape; (b) skewed shape caused by parallel shift of faces.

manner by translational symmetry. The crystal is formed by a three-dimensional stack of unit cells which is called the “crystal lattice” (Fig. 1.4). The unit cell is built up from three noncolinear vectors **a**, **b**, and **c**. In the general case, these vectors have unequal magnitudes and their mutual angles deviate from  $90^\circ$ . The arrangement of the molecule(s) in the unit cell may be asymmetrical, but very often it is symmetrical. This is illustrated in Figure 1.5 in two-dimensional lattices for rotational symmetries.

It follows from the combination of the lattice properties with rotational operations that in crystals only 1-, 2-, 3-, 4-, and 6-fold axes are allowed, and they can only occur among each other in a few certain combinations of angles as other angle orientations would violate the lattice properties. The number of all possible combinations reveals the 32 point groups, and delivers the deviation of the 32 point groups on the basis of the symmetry theory.

Adding an inversion center to the point group symmetry leads to the 11 Laue groups. These are of importance for the symmetry of X-ray diffraction patterns. Their symbols are: 1,  $2/m$ ,  $2/mmm$ , 3,  $3m$ ,  $4/m$ ,  $4/mmm$ ,  $6/m$ ,  $6/mmm$ ,  $m3$ , and  $m3m$ . Proteins and nucleic acids are chiral molecules and can, therefore, crystallize only in the 11 enantiomorphic point groups, as mentioned above.

The combination of point group symmetries with lattices leads to seven crystal systems, triclinic, monoclinic, orthorhombic, trigonal, tetragonal, hexagonal and cubic, the metric relationships of which are provided in Figure 1.6, with 14 different Bravais-lattice types which can be primitive, face-centered, all-face-centered, and body-centered (see Fig. 1.7). It is however possible to describe each translation lattice as a primitive lattice. Furthermore, different primitive unit cells can be chosen. Both situations are illustrated in Figure 1.8, where a two-dimensional (2D) face-centered tetragonal lattice is presented. The face-centered unit cell is assigned in the middle of the figure, and a primitive cell obeying the tetragonal symmetry has been marked by dashed lines. Three further putative primitive cells have been drawn in and numbered. Among these possible primitive unit cells or bases a so-called “reduced basis” **a**, **b**, **c** is important for the automated unit cell and space group determination of crystals from X-ray diffraction data. Such a basis is right-handed and the components of the metric tensor **G**

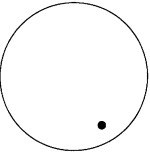
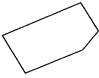

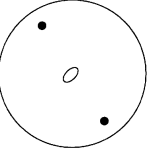
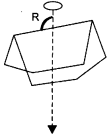

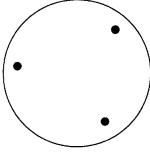
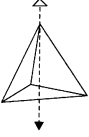

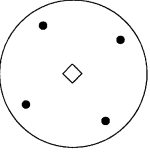
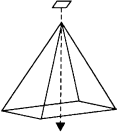

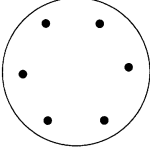
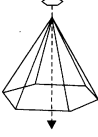
		symmetry framework	stereographic projection of the symmetry framework and of the general form	general form
$C_1$ triclinic-pedial pedion	1			
$C_2$ monoclinic-sphenoidal sphenoid	2			
$C_3$ trigonal-pyramidal trigonal pyramid	3			
$C_4$ tetragonal-pyramidal tetragonal pyramid	4			
$C_6$ hexagonal-pyramidal hexagonal pyramid	6			

Fig. 1.3 Graphical representation of the 11 enantiomorphic point groups.

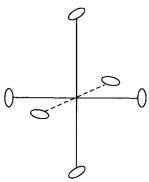
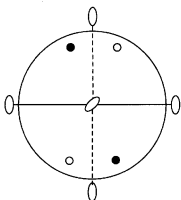

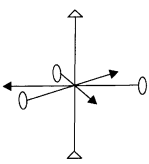
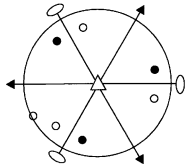

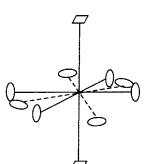
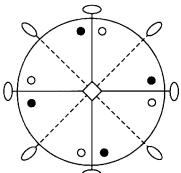
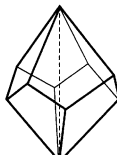
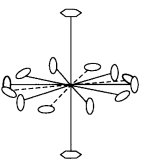
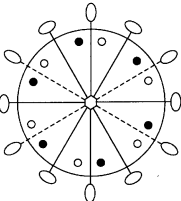
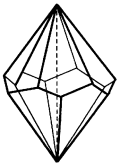
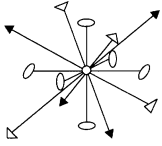
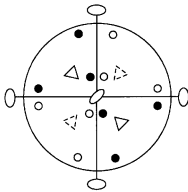
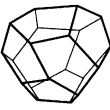
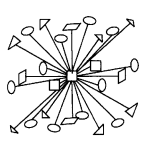
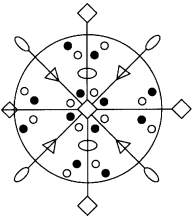
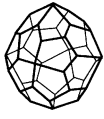
$D_2$ 222 orthorhombic-disphenoidal disphenoid			
$D_3$ 32 trigonal-trapezohedral trigonal-trapezohedron			
$D_4$ 422 tetragonal-trapezohedral tetragonal-trapezohedron			
$D_6$ 622 hexagonal-trapezohedral hexagonal-trapezohedron			
T 23 tetartoidal tetartoid			
O 432 gyroidal gyroid			

Fig. 1.3 (continued)

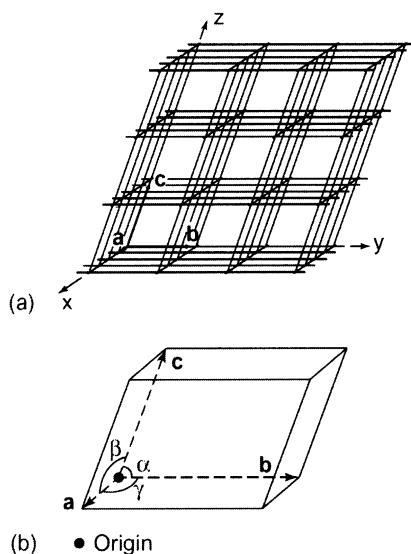


Fig. 1.4 (a) A crystal lattice; (b) a unit cell.

$$\begin{array}{lll} a \cdot a & b \cdot b & c \cdot c \\ b \cdot c & c \cdot a & a \cdot b \end{array}$$

(1.1)

satisfy special conditions listed in International Tables for Crystallography, Volume A, page 750 (Hahn, 2005).

Furthermore, additional symmetry elements are generated having translational components such as screw axes or glide mirror planes. There exist 230 space groups, of which 65 are enantiomorphic (for chiral molecules such as proteins); these are listed in Figure 1.9. As an example for such an additional symmetry element, the action of  $3_1$ - and  $3_2$ -screw axes is demonstrated in Figure 1.10. For a  $3_1$ -axis, the object is rotated by  $120^\circ$  anti-clockwise and shifted by one-third of the translation parallel to the direction of the axis. This is repeated twice, and the rotational start position is reached but shifted by one translational unit, thus generating a right-handed screw axis. For a  $3_2$ -axis, the object is again rotated by  $120^\circ$  anti-clockwise but shifted by two-thirds of the translation parallel to the direction of the axis. This is repeated twice and the rotational start position is reached but shifted by two translational units. The missing objects are obtained by applying the translation symmetry. The result is a left-handed screw axis. Figure 1.11 shows the graphical representation for the space group  $P2_12_12_1$  as listed in the International Tables for Crystallography (Hahn, 2005). The asymmetric unit is one-fourth of the unit cell, and can contain one or several molecules. Multimeric molecules may have their own symmetries which are called noncrystallographic symmetries. Here, axes which are 5-fold, 7-fold, etc., are also allowed.

It is useful to describe the relationship between a crystal face and its counterpart in the crystal lattice. Figure 1.12 a shows a crystal face in a general position inter-

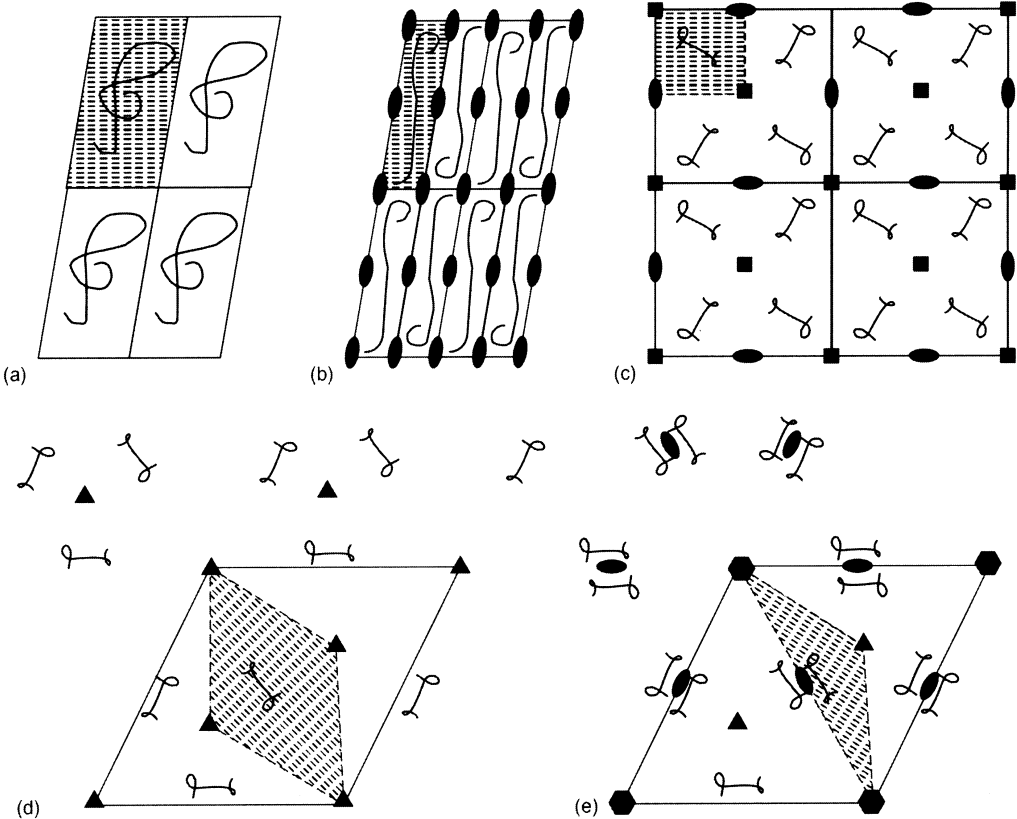


Fig. 1.5 Rotational symmetry elements in two-dimensional lattices: (a) 1, (b) 2, (c) 4, (d) 3, and (e) 6. The asymmetric unit is hatched.

Name	Possible Bravais Lattices	Axes of symmetry	Lattice
Triclinic	$P$	No axes of symmetry	$a \neq b \neq c$
Monoclinic	$P, C$	1 dyad axis (parallel to $b$ )	$a \neq b \neq c$
Orthorhombic	$P, C, I, F$	3 dyad axes mutually orthogonal	$a \neq b \neq c$
Tetragonal	$P, I$	1 tetrad axis (parallel to $c$ )	$a = b \neq c$
Trigonal	$P$	1 triad axis (parallel to $c$ )	$a = b \neq c$
	(or $R$ )		$a = b = c$
Hexagonal	$P$	1 hexad axis (parallel to $c$ )	$a = b \neq c$
Cubic	$P, I, F$	4 triad axes (along the diagonals of the cube)	$a = b = c$

Fig. 1.6 The seven crystal systems.



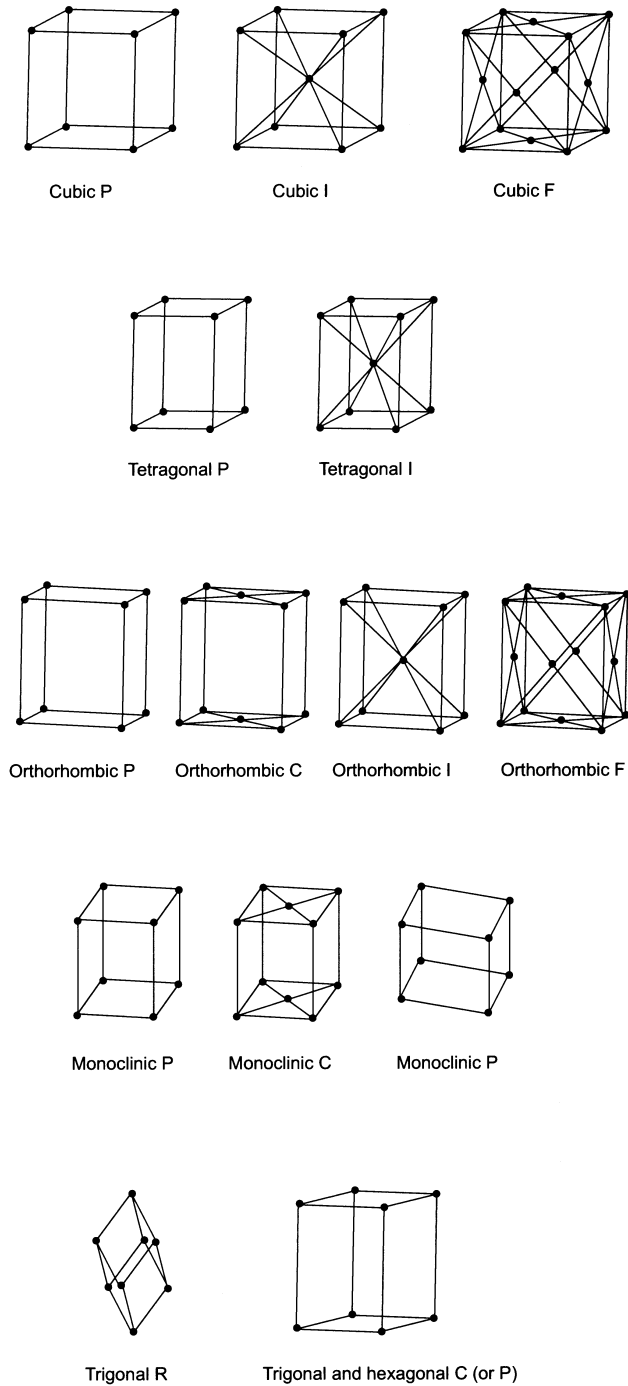


Fig. 1.7 The 14 Bravais lattices.

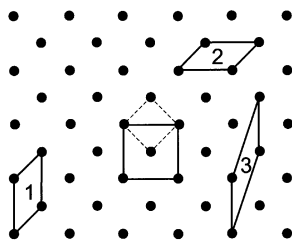


Fig. 1.8 Choice of different primitive unit cells.

secting the underlying coordinate system at distances  $OA$ ,  $OB$ ,  $OC$  on the  $a$ -,  $b$ -, and  $c$ -axes, respectively. Figures 1.12b and c depict the relevant crystal lattice, but only in two dimensions for the sake of clarity. The counterpart of crystal faces are the lattice planes. In Figure 1.12b the lattice planes have axis intercepts, which are in a ratio of  $2a$  to  $1b$ . In Figure 1.12c the ratio is  $2a$  to  $3b$ . In general, we have  $ma$ ,  $nb$ ,  $pc$  with the rational numbers  $m$ ,  $n$ , and  $p$ . In crystallography, it is not the axis intercepts but rather their reciprocal values which are used to characterize the position of a crystal face or lattice plane according to Eq. (1.2).

$$h : k : l = \frac{1}{m} : \frac{1}{n} : \frac{1}{p} . \quad (1.2)$$

The triple of numbers  $h$ ,  $k$ ,  $l$  is transformed in such a way that the numbers become integers and relatively prime. The  $hkl$  are called *Miller indices*, and can be applied to either crystal faces or lattice planes. The lattice planes are a stack of equidistant parallel planes with a lattice plane distance  $d(hkl)$ . The larger the *Miller indices* of a lattice plane, the smaller is  $d(hkl)$ .

Crystal system	Class	Point group symbols
Triclinic	1	$P1$
Monoclinic	2	$P2$ , $P2_1$ , $C2$
Orthorhombic	222	$C222$ , $P222$ , $P2_12_12_1$ , $P2_12_12$ , $P222_1$ , $C22_1$ , $F222$ , $I222$ , $I2_12_12_1$
Tetragonal	4	$P4$ , $P4_1$ , $P4_2$ , $P4_3$ , $I4$ , $I4_1$
	422	$P422$ , $P42_12$ , $P4_122$ , $P4_12_12$ , $P4_222$ , $P4_22_12$ , $P4_32_12$ , $P4_322$ , $I422$ , $I4_122$
Trigonal	3	$P3$ , $P3_1$ , $P3_2$ , $R3$
	32	$P312$ , $P321$ , $P3_121$ , $P3_112$ , $P3_212$ , $P3_221$ , $R32$
Hexagonal	6	$P6$ , $P6_5$ , $P6_4$ , $P6_3$ , $P6_2$ , $P6_1$
	622	$P622$ , $P6_122$ , $P6_222$ , $P6_322$ , $P6_422$ , $P6_522$
Cubic	23	$P23$ , $F23$ , $I23$ , $P2_13$ , $I2_13$
	432	$P432$ , $P4_132$ , $P4_232$ , $P4_332$ , $F432$ , $F4_132$ , $I432$ , $I4_132$

Fig. 1.9 The 65 enantiomorphic space groups.

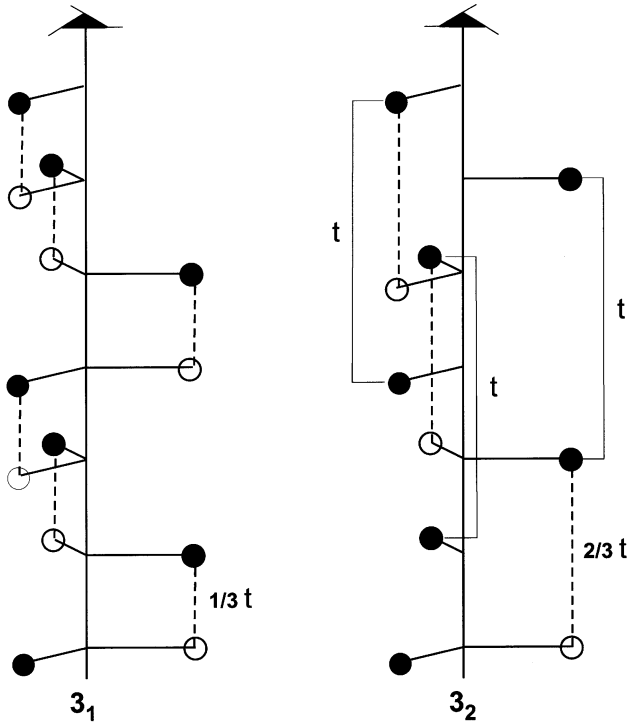


Fig. 1.10 Action of  $3_1$ - and  $3_2$ -screw axes.

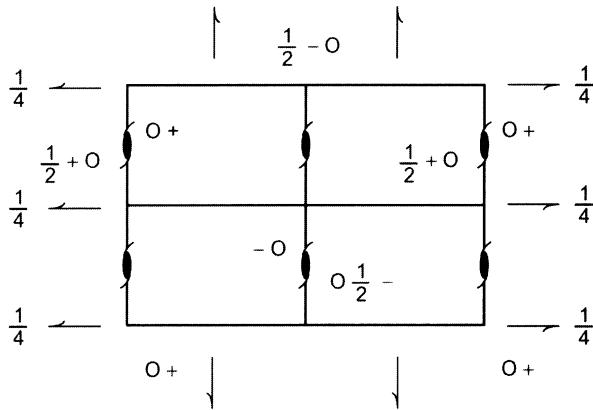
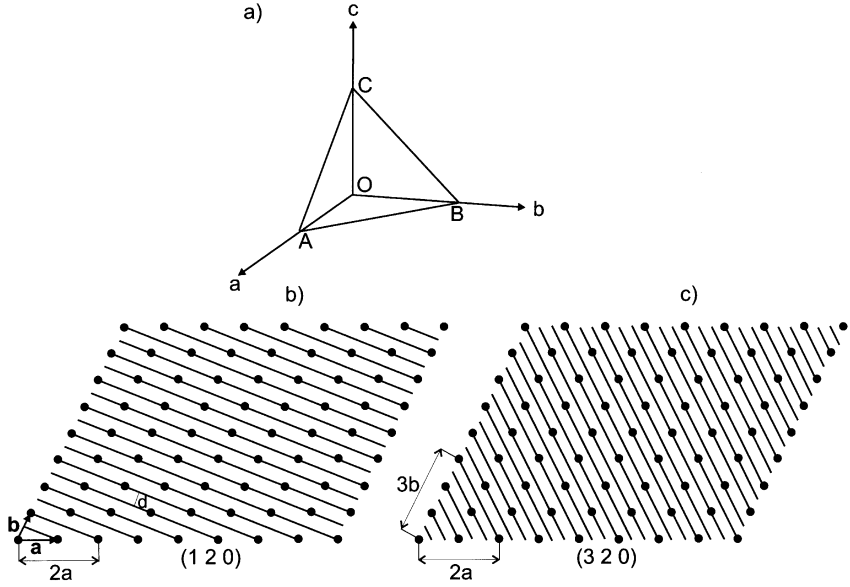


Fig. 1.11 Graphical representation of space group  $P2_12_12_1$ .



**Fig. 1.12** Relationship between a crystal face and lattice planes. (a) Axes intercepts of a crystal face; (b) corresponding 2D crystal lattice with lattice plane (120); and (c) with lattice plane (320).

The  $N$  atoms contained in a crystal unit cell are at positions

$$\mathbf{r}_j = x_j \mathbf{a} + y_j \mathbf{b} + z_j \mathbf{c} \quad (1.3)$$

for the atom  $j$  with the fractional coordinates  $x_j, y_j, z_j$ , whose absolute values are between 0 and 1, and the lattice vectors  $\mathbf{a}$ ,  $\mathbf{b}$ , and  $\mathbf{c}$ . The lattice vectors follow the metric of the crystal system to which the relevant crystal belongs. As the crystallographic crystal systems are adapted to the existent crystal symmetry, the analytical form of symmetry operations adopt very concise forms. Each coordinate triplet  $x'_j, y'_j, z'_j$  is related to the symmetry operation that maps a point with coordinates  $x, y, z$  onto a point with coordinates  $x'_j, y'_j, z'_j$ . The mapping of  $x, y, z$  onto  $x'_j, y'_j, z'_j$  is given by Eq. (1.4).

$$\mathbf{x}'_j = \mathbf{W} \mathbf{x}_j + \mathbf{w} \quad (1.4)$$

with

$$\mathbf{x}_j = \begin{pmatrix} x_j \\ y_j \\ z_j \end{pmatrix}, \quad \mathbf{x}'_j = \begin{pmatrix} x'_j \\ y'_j \\ z'_j \end{pmatrix}, \quad \mathbf{W} = \begin{pmatrix} W_{11} & W_{12} & W_{13} \\ W_{21} & W_{22} & W_{23} \\ W_{31} & W_{32} & W_{33} \end{pmatrix}, \quad \mathbf{w} = \begin{pmatrix} w_1 \\ w_2 \\ w_3 \end{pmatrix}. \quad (1.5)$$

$\mathbf{W}$  is called the rotation part and  $\mathbf{w}$  the translation part. In Figure 1.11, for example, the  $z_1$ -axis parallel  $\mathbf{c}$  going through  $x = 1/4, y = 0$  maps coordinates  $x, y, z$  onto  $-x + 1/2, -y, z + 1/2$  with

$$\mathbf{W} = \begin{pmatrix} -1 & 0 & 0 \\ 0 & -1 & 0 \\ 0 & 0 & 1 \end{pmatrix} \quad \text{and} \quad \mathbf{w} = \begin{pmatrix} 1/2 \\ 0 \\ 1/2 \end{pmatrix} \quad (1.6)$$

which can be verified by matrix multiplication.

## 1.2

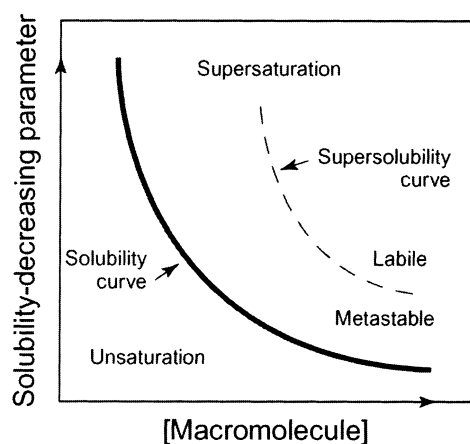
### Protein Solubility

Figure 1.13 shows a typical phase diagram illustrating the solubility properties of a macromolecule. In the labile phase crystal nucleation and growth compete, whereas in the metastable region only crystal growth appears. In the unsaturated region the crystals dissolve. The solubility of proteins is influenced by several factors, as follows.

#### 1.2.1

##### Ionic Strength

A protein can be considered as a polyvalent ion, and therefore its solubility can be discussed on the basis of the Debye–Hückel theory. In aqueous solution, each ion is surrounded by an “atmosphere” of counter ions. This ionic atmosphere influences the interactions of the ion with water molecules and hence the solubility.



**Fig. 1.13** Phase diagram illustrating the solubility properties of macromolecules. (Reproduced by permission of Academic Press, Inc., from Weber, 1997.)

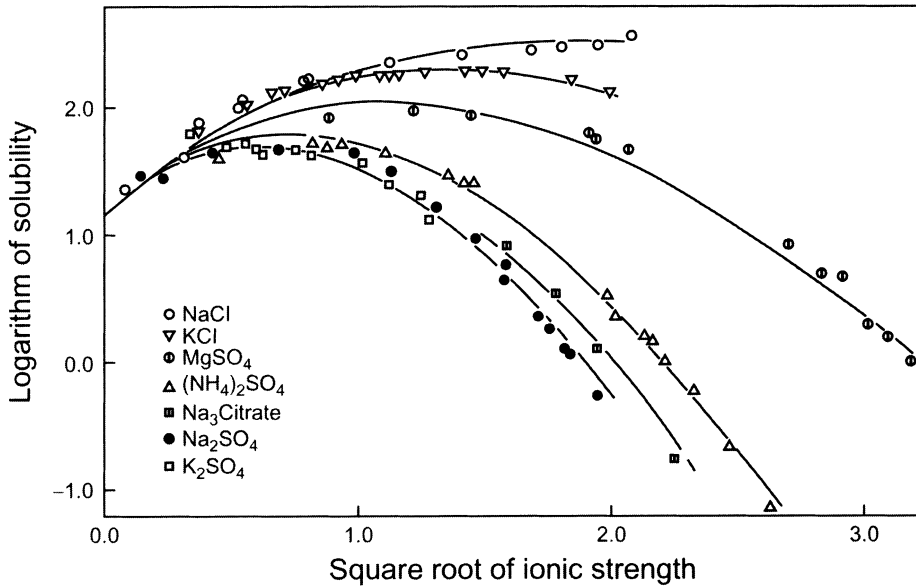
## 1.2.1.1 “Salting-in”

At low ionic concentration, the “ionic atmosphere” increases the solubility as it increases the possibilities for favorable interactions with water molecules. Thus, we obtain Eqs. (1.7) and (1.8):

$$\log S - \log S_0 = \frac{AZ_+Z_-\sqrt{\mu}}{1 + aB\sqrt{\mu}} \quad (1.7)$$

$$\mu = \frac{1}{2} \sum c_j Z_j^2 \quad (1.8)$$

where  $\mu$ =ionic strength,  $S$ =solubility of the salt at a given ionic strength  $\mu$ ,  $S_0$ =solubility of the salt in absence of the electrolyte,  $Z_+$ ,  $Z_-$  the ionic charge of salt ions,  $A$ ,  $B$ =constants depending on the temperature and dielectric constant,  $a$ =average diameter of ions, and  $c_j$ =concentration of the  $j$ th chemical component. Ions with higher charge are more effective for changes in solubility. Most salts and proteins are more soluble in low ionic strength than in pure water; this is termed “salting-in” (Fig. 1.14).



**Fig. 1.14** Solubility of carboxyhemoglobin in various electrolytes at 25 °C. (Reproduced by permission of the American Society for Biochemistry and Molecular Biology, from Green, 1932.)

### 1.2.1.2 “Salting-out”

At higher ionic strength the ions compete for the surrounding water, and consequently the water molecules are taken away from the dissolved agent and the solubility decreases according to Eq. (1.9):

$$\log S - \log S_0 = \frac{AZ_+Z_- \sqrt{\mu}}{1 + aB\sqrt{\mu}} - K_s\mu \quad (1.9)$$

The term  $K_s\mu$  predominates at high ionic strengths, which means that “salting-out” is then proportional to the ionic strength (Fig. 1.14). In a medium with low ionic strength, the solubility of a protein can be decreased by increasing or decreasing the salt concentration. Salts with small, highly charged ions are more effective than those with large, lowly charged ions. Ammonium sulfate is often used because of its high solubility.

## 1.2.2

### pH and Counterions

The more soluble a protein, the larger is its net charge, with the minimum solubility being found at the isoelectric point. The net charge is zero, and hence the packing in the solid state (in the crystal) is possible owing to electrostatic interactions without the accumulation of a net charge of high energy. All “salting-out” curves are parallel,  $K_s$  remains constant, and  $S_0$  varies with pH (Fig. 1.15 a and b). In some cases the isoelectric point is different at low and high ionic strengths, owing to interactions of the protein with counterions which can cause a net charge at the pH of the isoelectric point.

## 1.2.3

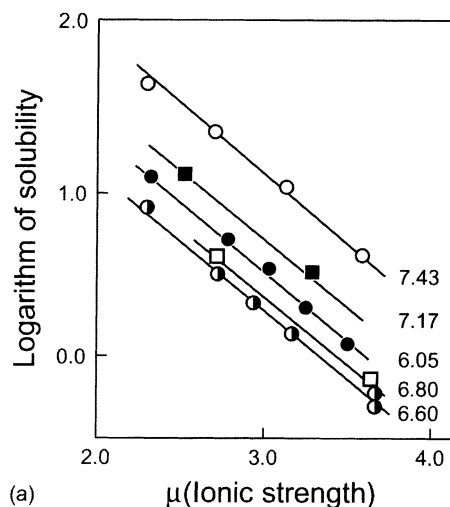
### Temperature

Many factors governing protein solubility are temperature-dependent. The dielectric constant decreases with increasing temperature. In the solution energy,  $\Delta G = \Delta H - T\Delta S$ , the entropy term has an increasing influence with increasing temperature. The temperature coefficient of the solubility depends on other conditions (ionic strength, presence of organic solvents, etc.). At high ionic strength most proteins are less soluble at 25 °C than at 4 °C – that is, the temperature coefficient is negative. The opposite is valid for low ionic strength.

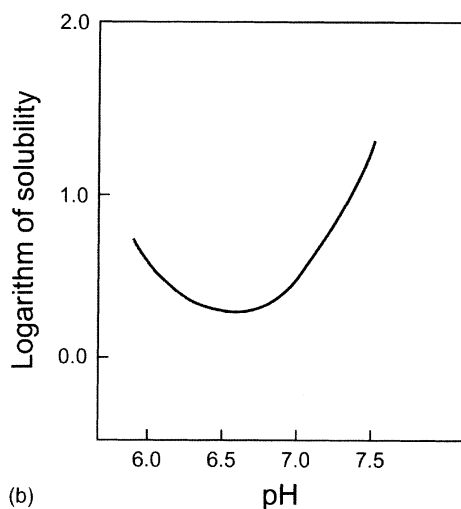
## 1.2.4

### Organic Solvents

The presence of organic solvents leads to a decrease in the dielectric constant. This causes an augmentation of the electric attraction between opposite charges on the surface of the protein molecule, and hence to a reduction in solubility. In general, the solubility of a protein is reduced in the presence of an organic



**Fig. 1.15** (a) Solubility of hemoglobin at different pH values in concentrated phosphate buffers; (b) extracted from (a). (Reproduced by permission of the American Society for Biochemistry and Molecular Biology, from Green, 1931.)



solvent if the temperature decreases. Often, organic solvents denature proteins, and consequently one should work at low temperatures.

### 1.3

#### Experimental Techniques

The whole field of macromolecular crystallography has been excellently reviewed in Volumes 114 and 115 and Volumes 276 and 277 of *Methods in Enzymology*. A collection of review articles concerning the theory and practice of crys-



tallization of biomacromolecules is provided in Part A of Carter and Sweet (1997).

A protein preparation to be used in crystallization studies should be “pure” or “homogeneous” at a level that established chromatographic methods are providing (protein content  $\geq 95\%$ ). Furthermore, it should meet the requirements of “structural homogeneity”. These requirements can be enumerated as follows. It is first necessary to prepare the protein in an isotypically pure state free from other cellular proteins. It may then be necessary to maintain the homogeneity of the protein preparation against covalent modification during crystallization by adding inhibitors of sulfhydryl group oxidation, proteolysis and the action of reactive metals. It may be necessary to suppress the slow denaturation/aggregation of the protein and to restrict its conformational flexibility to reduce the entropic barrier to crystallization presented by extensive conformational flexibility. For the crystallization of biomacromolecules, a broad spectrum of crystallization techniques exists, the most common of which are described here.

### 1.3.1

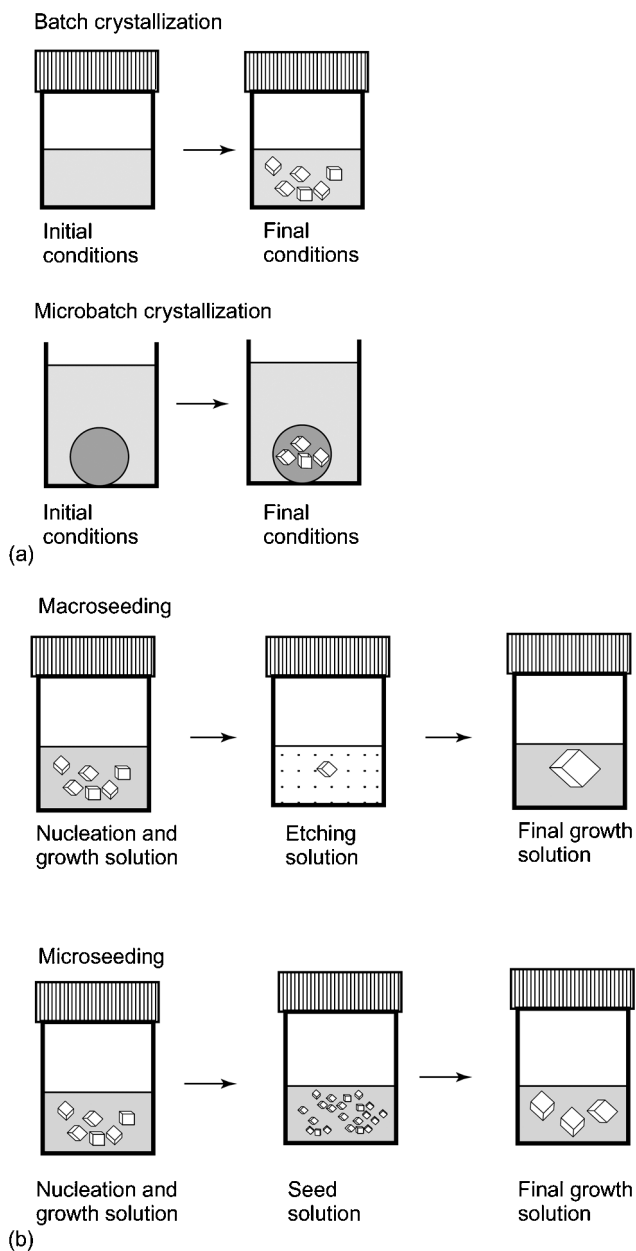
#### **Batch Crystallization**

This is the oldest and simplest method (see Fig. 1.16a). In batch experiments, vials containing supersaturated protein solutions are sealed and left undisturbed. In microbatch methods, a small (2–10  $\mu\text{L}$ ) droplet containing both protein and precipitant is immersed in an inert oil which prevents droplet evaporation. In the case that ideal conditions for nucleation and growth are different, it is useful to undertake the separate optimization of these processes. This can be done by seeding – a technique where crystals are transferred from nucleation conditions to those that will support only growth (Fig. 1.16b). For macroseeding, a single crystal is transferred to an etching solution, then to a solution of optimal growth. In microseeding experiments, a solution containing many small seed crystals, occasionally obtained by grinding a larger crystal, is transferred to a crystal growth solution.

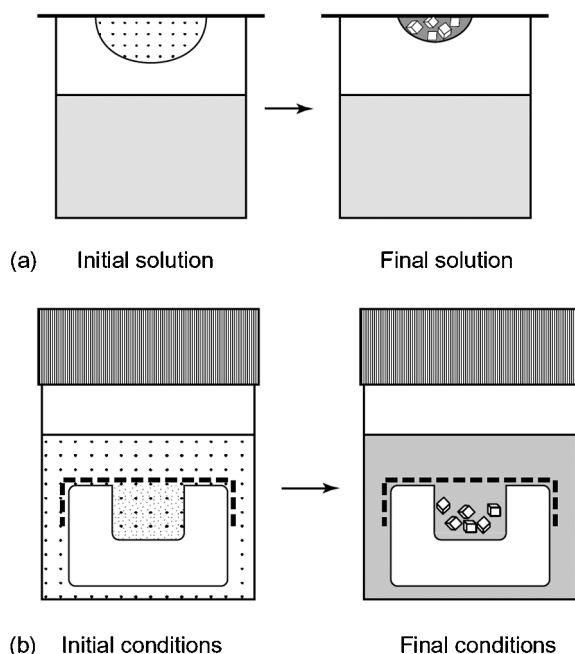
### 1.3.2

#### **Vapor Diffusion**

Crystallization by vapor diffusion is depicted in Figure 1.17a. Here, unsaturated precipitant-containing protein solutions are suspended over a reservoir. Vapor equilibration of the droplet and reservoir causes the protein solution to reach a supersaturation level where nucleation and initial crystal growth occur. Changes in soluble protein concentration in the droplet are likely to decrease supersaturation over the time course of the experiment. The vapor diffusion technique can be carried out as either a hanging drop or sitting drop method.



**Fig. 1.16** Schematic presentation of (a) batch crystallization and (b) seeding techniques. (Reproduced by permission of Academic Press, Inc., from Weber, 1997.)



**Fig. 1.17** Schematic representation of (a) vapor diffusion and (b) dialysis. (Reproduced by permission of Academic Press, Inc., from Weber, 1997.)

### 1.3.3

#### Crystallization by Dialysis

In crystallization by dialysis, the macromolecular concentration remains constant, as in batch methods (Fig. 1.17b) because the molecules are forced to stay in a fixed volume. The solution composition is changed by diffusion of low-molecular-weight components through a semipermeable membrane. The advantage of dialysis is that the precipitating solution can be easily changed. Dialysis is also uniquely suited to crystallizations at low ionic strength and in the presence of volatile reagents such as alcohols.

## 1.4

### Crystallization Screenings

Screening schemes have been developed which change the most common parameters of this multiparameter problem, such as protein concentration, the nature and concentration of the precipitant, pH, and temperature. Each screening can be extended by adding specific additives in low concentrations that affect the crystallization. Sparse matrix crystallization screens are widely applied. The

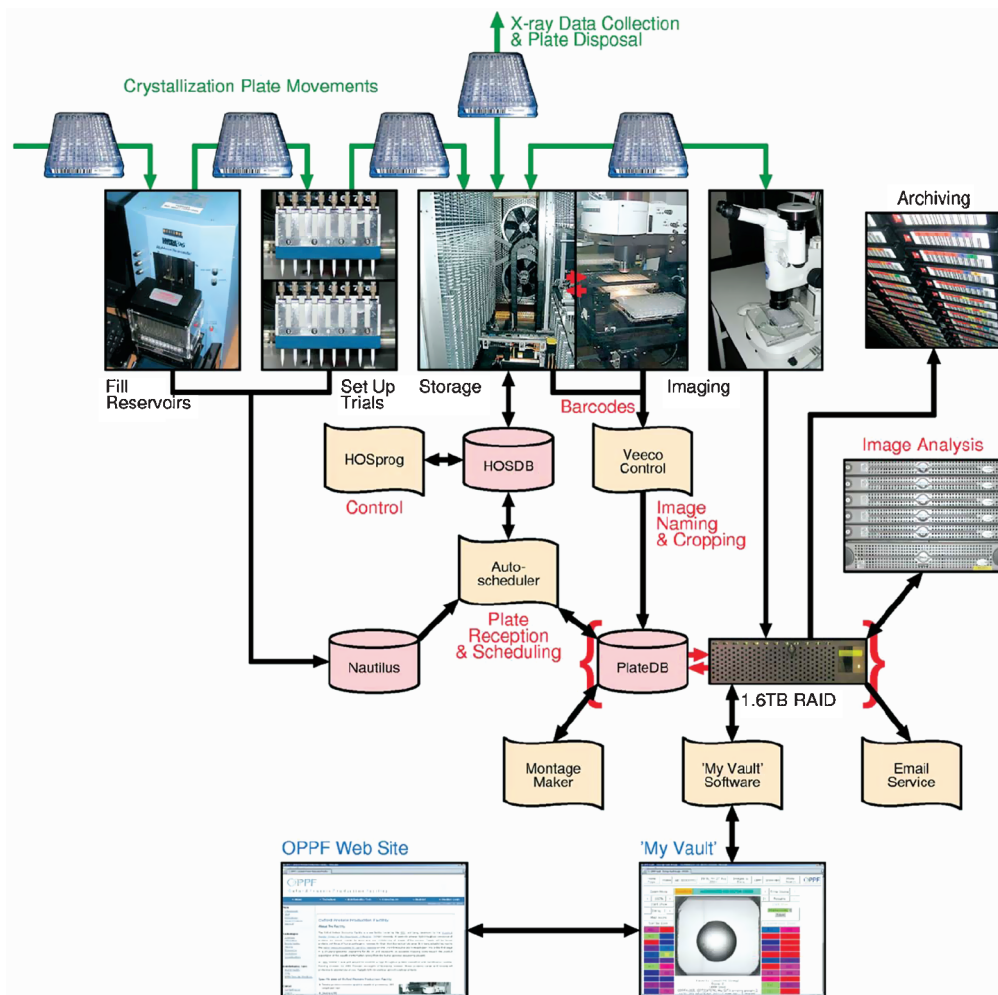
sparse matrix formulation allows the efficient screening of a broad range of the most popular and effective salts (e.g., ammonium sulfate, sodium and potassium phosphate, sodium citrate, sodium acetate, lithium sulfate), polymers [e.g., poly(ethyleneglycol) (PEG) of different molecular masses (from 400 to 8000)], and organic solvents [e.g., 2,4-methylpentanediol (MPD), 2-propanol, ethanol) versus a wide range of pH. Another approach is the systematic screening of the statistically most successful precipitants. A single precipitant is screened at four unique concentrations versus seven precise levels of pH between 4 and 10. Such grid screens can be carried out with ammonium sulfate, PEG 600, MPD, and PEG 6000 in the presence of 1.0 M lithium chloride or sodium chloride. For the crystallization of membrane proteins (see Michel, 1991) for each detergent which is necessary to solubilize the membrane protein, a whole grid screen or sparse matrix screen must be constructed. In principle, all three techniques can be applied for the different screening schemes, but in the most part the vapor diffusion technique is applied because it is easy to use and the protein consumption is low. For a typical broad screening, about 2 mg of protein is sufficient. Chryschem plates (sitting drop) or Linbro plates (hanging drops) may be used for the vapor diffusion crystallization screening experiments. Once crystals have been obtained, their size and quality can be optimized by additional fine screens around the observed crystallization conditions. There are no general rules to indicate which method should be used to crystallize which type of protein; however, suggestions for crystallization conditions to be tested can be obtained from the Biological Macromolecule Crystallization Database (Gilliland et al., 1994; <http://xpdn.nist.gov:8080/bmcd/bmcd.html>).

## 1.5

### High-Throughput Crystallization, Imaging, and Analysis

During recent years, the sequencing of whole genomes from bacteria to higher organisms, including man, has opened up the systematic determination of their gene products. Today, this new field is known as “structural genomics” or “structural proteomics”. Structural genomics represents not only the structure determination of gene products, by using the old approach of structural biology, one target, one researcher, but also comprises the creation and application of high-throughput techniques. Unfortunately, these major efforts can be managed only by larger consortia, and several such set-ups have been established in the USA, Japan, and Europe. A complete list can be found on the Internet under [http://sg.pdb.org/target\\_centers.html](http://sg.pdb.org/target_centers.html). The automation includes the whole workflow in protein structure determination from cloning, expression, purification, quality assessment, crystallization, imaging, X-ray data collection, and structure analysis.

The focus of the following section is on high-throughput crystallization, crystal imaging, and image analysis. Today, crystallization robots have been developed that not only automate the crystallization set-ups but also reduce the vol-



**Fig. 1.18** Scheme of the components and workflow of the OPPF high-throughput crystallization facility. Green arrows show the transfer of 96-well crystallization plates between robots. The flow of images and control data is shown by black arrows. Databases are indicated by pale red “disk

cylinders” and specific sections of the control software are represented by orange “paper”. The method of interaction with the web interface is indicated by sample web pages. (Reproduced by permission of Elsevier Ltd., from Mayo et al., 2005.)

ume of the dispensed protein drops from  $\mu\text{L}$  quantities to 50 nL. This dramatically increases the number of screening conditions with the same amount of available protein. Several facilities have been set up, which have completely automated the liquid and protein dispensing, the plate storage, imaging, and image analysis. A number of these systems are now also available commercially.

In principle, all systems contain the same components, and in the following section a typical large-scale facility installed at the Oxford Protein Production Facility (OPPF) is described in more detail (Fig. 1.18). The initial crystallization screening uses a panel of 480 conditions selected from standard (commercially available) crystallization kits. The kits are reformatted into 96-deep well “Master blocks” by a Qiagen Biorobot 8000. Pre-barcoded 96-well crystallization plates (Greiner Bio-One Ltd, UK) are used for the trials, the precipitant being transferred from the master blocks to the reservoirs using a Hydra-96 microdispenser (Matrix Technologies Ltd, UK). The barcode of the plate is then read and transferred to the LIMS (Laboratory Information Management System). The plate is then placed on a Cartesian Technologies Microsys MIC400 (Genomic Solutions Ltd, UK) where a 100-nL drop of protein solution is placed on the central position of each crystallization shelf and mixed with 100 nL of the corresponding reservoir. The pipetted plates are sealed and stored in an automated storage vault (The Automated Partnership Ltd, UK). Imaging is performed using an Oasis 1700 automatic imaging system (Veeco, UK), which is housed in an annex to the storage vault. Plates can be picked by a robot arm in the storage vault and transferred to the imaging system controlled by the LIMS. In this way, a 96-well plate can be imaged in 40 s. The digitized images are transferred to a RAID storage system, and each well image is classified using the York crystal image analysis software (Wilson, 2004). The program assigns different scores to the images, ranging from 0 for insignificant objects, such as those due to shadows at the edge of the drop, to 6 for good single crystals. Figure 1.18 also shows the components and arrangement of the computer hardware and LIMS.

## References

- Carter, C.W. Jr, Sweet, R.M. (Eds.), *Macromolecular Crystallography*, Part A, *Methods Enzymol.* **1997**, 276, 1–700.
- Carter, C.W. Jr, Sweet, R.M. (Eds.), *Macromolecular Crystallography*, Part B, *Methods Enzymol.* **1997**, 277, 1–664.
- Gilliland, G.L., Tung, M., Balkeslee, D.M., Ladner, J.E. *Acta Crystallogr.* **1994**, D50, 408–413.
- Green, A.A. *J. Biol. Chem.* **1931**, 93, 495–516.
- Green, A.A. *J. Biol. Chem.* **1932**, 95, 47–66.
- Hahn, T. (Ed.), *International Tables for Crystallography*, Volume A, Springer, Dordrecht, **2005**.
- Mayo, C.J., Diprose, J.M., Walter, T.S., Berry, I.M., Wilson, J., Owens, R.J., Jones, E.Y., Harlos, K., Stuart, D.I., Esnouf, R.M. *Structure* **2005**, 13, 175–182.
- Michel, H. (Ed.), *Crystallization of Membrane Proteins*, CRC Press, Boca Raton, **1991**.
- Weber, P.C. *Methods Enzymol.* **1997**, 276, 13–23.
- Wilson, J. *Cryst. Rev.* **2004**, 10, 73–84.